PERGAMON

International Journal of Heat and Mass Transfer 42 (1999) 4143–4152

International Journal of HEAT and MASS TRANSFER

www.elsevier.com/locate/ijhmt

Optimization of the inlet velocity profile for uniform epitaxial growth in a vertical metalorganic chemical vapor deposition reactor

W.K. Cho, D.H. Choi*, M.-U. Kim

Department of Mechanical Engineering, Korea Advanced Institute of Science and Technology, Taejon 305-701, South Korea

Received 2 October 1998; received in revised form 12 February 1999

Abstract

An optimization procedure is devised to find the inlet velocity profile that yields as uniform an epitaxial layer as possible in a vertical MOCVD reactor. It involves the solution of fully elliptic equations of motion, temperature, and concentration; the process is highly nonlinear and has been efficiently treated by breaking it into a series of linear problems. The optimal profile approximated by a 6th-degree Chebyshev polynomial is very successful in reducing the spatial non-uniformity of the growth rate. The optimization is particularly effective when the Reynolds number is high and the inlet-to-wafer distance becomes large. It is also found that a properly constructed inlet velocity profile can suppress the buoyancy driven secondary flow and improve the growth-rate uniformity. © 1999 Elsevier Science Ltd. All rights reserved.

1. Introduction

Epitaxial (single crystalline) thin film is the basic material for manufacturing compound semi-conductors (e.g. GaAs). Among various methods commonly used in growing thin films, such as molecular beam epitaxy (BME), liquid phase epitaxy (LPE) and metalorganic chemical vapor deposition (MOCVD), the MOCVD process through pyrolysis or chemical reaction of vapor-phase source has been most popular because of the highly uniform film thickness and composition [1,2] that it produces.

The epitaxial layer grown in a vertical MOCVD reactor is generally satisfactory for many practical purposes. However, it may fall short of meeting the required thickness uniformity for very demanding applications such as the micro-electronics technique. As the mass transfer of the source gas governs (mass-transport-limited regime) [3–9] the deposition rate for conventional operating condition (0.1–1 atm, 800–1100 K), a sensible way to improve the deposition performance is to control the flow phenomena in a reactor under such circumstances. Many techniques have been proposed in the literature in this regard. Among these are rotating the reacting surface [3–5], lowering the reactor pressure or reversing the flow direction to suppress the buoyancy effects [4,5], revising reactor shapes [4,10], and controlling the inlet flow condition [8,9,11,12]. A popular practice is to use the flow-distributor of porous materials [3,5,8] at the inlet to make the inlet velocity distribution uniform in the belief that a uniform flux yields even growth rate across the wafer. This, however, is not completely true. Although it does help achieve generally uniform film thickness, the accelerating flow around the susceptor edge inevi-

* Corresponding author. Tel.: +82-42-869-3018; fax: +82-42-869-3210.

E-mail address: dhchoi@hanbit.kaist.ac.kr (D.H. Choi)

0017-9310/99/$ - see front matter © 1999 Elsevier Science Ltd. All rights reserved.
PII: S0017-9310(99)00085-X

Nomenclature

A	area
C	concentration
E	cost function
G	growth rate
Gr	Grashof number, $Gr = g\beta(T_s - T_{in})r_s^3/\nu^2$
H	wafer to inlet height
M	molecular weight
N	degree of polynomial
Pr	Prandtl number, $Pr = \nu/\alpha_T$
R	reactor radius
Re	Reynolds number, $Re = u_{in} r_s/\nu$
Re_Ω	rotational Reynolds number, $Re_\Omega = \Omega r_s^2/\nu$
Sc	Schmidt number, $Sc = \nu/\alpha_M$
T	temperature
$\mathbf{V}$	velocity vector
a	polynomial coefficients
g	gravity
n	unit normal vector
p	pressure
(r, x)	radial and axial coordinates
u	velocity components

Greek symbols

Ω	angular velocity
α	diffusion coefficient
β	thermal expansion coefficient
δ	small displacement
ϕ	Chebyshev polynomials
ρ	density
ν	kinematic viscosity

Subscripts and superscripts

*	dimensional quantity
M	mass
T	temperature
in	inlet
(r, x)	radial and axial coordinates
s	susceptor
w	wafer

tably results in higher growth rate at the wafer edge than in the center [3,4,8].

The recent study by Cho et al. [9] showed that the uniformity of the film can be greatly enhanced by controlling the concentration distribution at the inlet. Taking full advantage of the linearity of the system, the procedure to determine the optimal inlet condition was made fairly efficient as the costly iteration for the flow-field calculation could be avoided. While the scheme is promising, controlling the inlet concentration is not easy and thus may lack practicality. To make the procedure more practical, one should consider controlling other quantities, such as the inlet velocity or the chamber shape. Obviously, it makes the system nonlinear and devising an efficient optimization process become much more complex.

The analysis is much more involved because the relation between the inlet velocity and the growth rate is nonlinear as shall be seen later in this paper. Once the optimal inlet velocity is found, it can be readily implemented by using the existing methods such as the flow distributor of porous material [8] or the multiple gas-injector technique [11,12]. The method would be economically attractive as it does not require any complex and/or expensive equipments such as a vacuum pump to reduce the operating pressure or a motor to rotate the susceptor. As an extension of the earlier study, the major objective of the present study is to develop such procedure and to perform analyses to obtain optimal inlet velocity profiles for various aspect ratios and flow/thermal conditions.

2. Analysis method

In the chamber of cylindrical shape considered in the present study, the susceptor of radius r_s is a distance H away from the inlet of radius r_{in} at the top (see Fig. 1); the reactant gas is blown in through the inlet and goes out via the gap between the chamber wall and the susceptor. Since the flow is axisymmetric, the governing equations of continuity, momentum, energy and concentration in (r, x) coordinates may be written as:

$$\frac{1}{r}\frac{\partial}{\partial r}(ru_r) + \frac{\partial}{\partial x}(u_x) = 0 \tag{1}$$

$$(\mathbf{V}\nabla)u_r = -\frac{\partial p}{\partial r} + \frac{1}{Re}\left(\nabla^2 u_r - \frac{u_r}{r^2}\right) \tag{2}$$

$$(\mathbf{V}\nabla)u_x = -\frac{\partial p}{\partial x} + \frac{1}{Re}\nabla^2 u_x - \frac{Gr}{Re^2}T \tag{3}$$

$$(\mathbf{V}\nabla)T = \frac{1}{RePr}\nabla^2 T \tag{4}$$

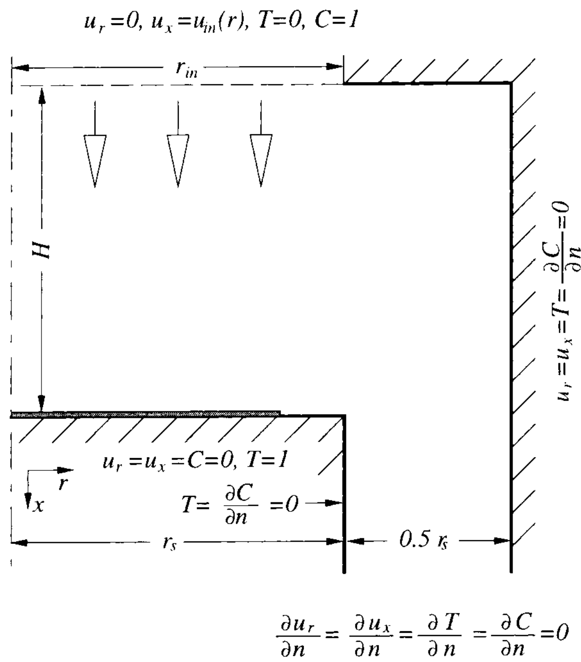

Fig. 1. Schematic of a vertical reactor.

$$(\mathbf{V}\nabla)C = \frac{1}{ReSc}\nabla^2 C \tag{5}$$

where $(u_r,\ u_x)$ are velocity components in $(r,\ x)$ directions, respectively, p the total hydrostatic pressure, T the temperature, and C the concentration. It suffices to consider one component for concentration since only the gallium containing species, $Ga(CH_3)_3$, limits the GaAs epitaxial layer growth rate [3–8]. These equations have been made dimensionless by using the mean inlet velocity u_{in}, the temperature difference $\Delta T(=T_s-T_{in})$, the inlet reactant gas concentration C_{in} and the susceptor radius r_s. The dimensionless parameters Re $(=u_{in}r_s/\nu)$, Gr $(=g\beta(T_s-T_{in})r_s^3/\nu^2)$, Pr $(=\nu/\alpha_T)$ and Sc $(=\nu/\alpha_M)$ are Reynolds number, Grashof number, Prandtl number, and Schmidt number, where $\nu,\ \beta,\ \alpha_T$ and α_M denote the kinematic viscosity, the thermal expansion coefficient, the thermal diffusivity and the mass diffusivity, respectively. Note that the Bussinesq approximation is invoked for the buoyancy term in the momentum equation and the concentration gradient is assumed to have little impact on density variation because the reactant mole fraction is negligibly small (typically $10^{-5} \sim 10^{-3}$).

For the computational domain that extends from the inlet to the exit in one azimuthal plane (see Fig. 1), the following boundary conditions appear to simulate the real situation best:

Inlet (given)

$$u_r = 0, \quad u_x = u_{in}(r)$$

$$T = 0, \quad C = 1 \tag{6}$$

Exit

$$\frac{\partial u_r}{\partial x} = \frac{\partial u_x}{\partial x} = \frac{\partial T}{\partial x} = \frac{\partial C}{\partial x} = 0, \quad \frac{\partial p}{\partial x} = \text{const} \tag{7}$$

Axis (symmetry)

$$u_r = 0, \quad \frac{\partial u_x}{\partial r} = \frac{\partial p}{\partial r} = \frac{\partial T}{\partial r} = \frac{\partial C}{\partial r} = 0 \tag{8}$$

Solid surface

$$u_r = u_x = \frac{\partial p}{\partial n} = 0 \tag{9}$$

$$T = 1, \quad C = 0 \quad \text{(wafer surface)}$$

$$T = \frac{\partial C}{\partial n} = 0 \quad \text{(other surface)}$$

The vanishing concentration at the wafer surface [3–9] is the result of the deposition process that accompanies the chemical reaction. Also, since the amount of mass deposition compared with the flow rate is negligible, the mass-depletion effects are not considered.

On a non-staggered grid, the governing equations, Eqs. (1)–(5), subject to the boundary conditions (6)–(9) are solved by SIMPLE algorithm of Patankar [13]. The diffusive derivatives in the equations are discretized by the central differencing while the convective derivatives are done by QUICK scheme [14]. The momentum interpolation scheme of Rhie and Chow [15] is incorporated in the procedure to avoid the occurrence of the unrealistic checker-board pressure pattern. The process is iterative and the solution is considered to have converged when the sum of the residuals over the entire domain in each equation becomes less than 10^{-5}.

3. Optimization technique

We wish to make the spatial variation of the deposition rate as small as possible by controlling the inlet velocity distribution. The film growth rate in a mass-transport-limited regime is expressed by Fick's law as

$$G^* = -\alpha_M \frac{\partial C^*}{\partial x^*} \frac{M_F}{\rho_F} \tag{10}$$

where M_F is the molecular weight, ρ_F the density of the growing solid film and the superscript * denotes the dimensional quantity. The nondimensionalization

by $G = G^* \times (r_s\rho_F / C_{in}\alpha_M M_F)$ results in $G = \partial C/\partial x$ in that the growth rate is identical to the normal concentration gradient on the wafer.

The cost function representing the normalized spatial non-uniformity of the growth rate that needs to be minimized may be defined as

$$E = \left\{ \frac{\int_{A_w} [G(r) - \bar{G}]^2 \, dA}{\bar{G}^2 A_w} \right\}^{1/2} \quad (11)$$

where $\bar{G}$ is the average growth rate and A_w is the area of the wafer whose radius is taken to be 0.8 times that of susceptor's. The wafer size is arbitrary and could take a larger or smaller value. Taking this value close to 1, however, is neither practical nor meaningful as the integral is dominated by the outer region where G cannot be kept uniform anyway.

The inlet velocity profile may be approximated by a linear combination of basis functions $\phi_k(r)$ as

$$u_{in}(r) = \sum_{k=0}^{N} a_k \phi_k(r) \quad (12)$$

where N is the degree of functions used. Taking advantage of symmetry, we choose the Chebyshev polynomial of even degree as the basis function in view of its orthogonality and excellent properties of approximating functions. The objective now becomes to find the set of coefficients a_k in Eq. (12) that minimizes the cost function E. The process is referred to as 'reduced basis method' [16] and is far more efficient and/or accurate than seeking the velocity distribution itself at discrete node points across the inlet in which the comparable accuracy can only be achieved with a great deal more computational effort.

To tackle the nonlinear relation between the cost function and the design variable, an approach known as 'sequential linear programming (SLP)' [16] is adopted: Consider the present nonlinear programming problem to minimize Eq. (11) which is a function of $\mathbf{a}$. Using the first order Taylor expansion about point $\mathbf{a}^0$, the cost function at $\mathbf{a}$ $(= \mathbf{a}^0 + \delta\mathbf{a})$ can be written as

$$E(\mathbf{a}) \approx E(\mathbf{a}^0) + \nabla E(\mathbf{a}^0)\delta\mathbf{a} \quad (13)$$

Rather than dealing directly with this equation to find $\delta\mathbf{a}$, it is more convenient and makes more sense to work with the growth rate $G(\mathbf{a})$ since G is more sensitive to the flow field and, thus, to $\mathbf{a}$ than E is. In other words, the direction and the magnitude of $\delta\mathbf{a}$ that minimizes E can be found more effectively by Eq. (11) with G as an intermediate variable than by Eq. (13) alone. To implement this idea, we first linearize the growth rate as was done for E in Eq. (13):

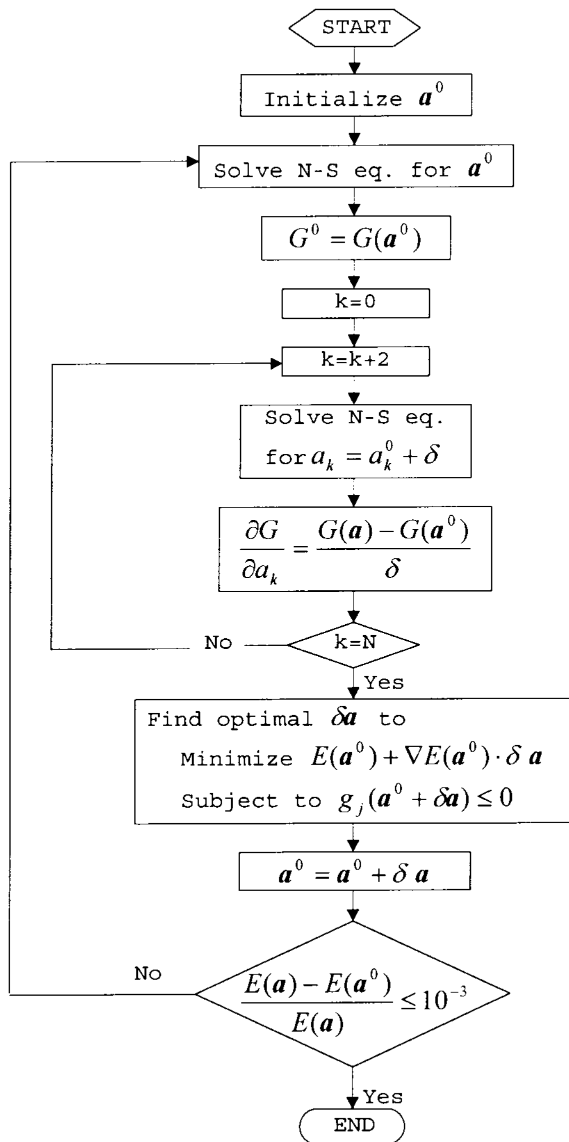

Fig. 2. Flow chart of the optimization procedure.

$$G(\mathbf{a}) \approx G(\mathbf{a}^0) + \nabla G(\mathbf{a}^0)\delta\mathbf{a} \quad (14)$$

This, together with Eq. (11), is used to evaluate the cost function after each change in $\mathbf{a}$ is made. The approach is very efficient in finding $\delta\mathbf{a}$ and makes the whole optimization procedure computationally affordable as the number of passes through the time-consuming flow analysis loop can be kept minimum. The procedure is outlined in Fig. 2; the optimum state is considered achieved when the relative variation in E becomes less than 10^{-3}. Fig. 3 provides a geometric interpretation of the SLP to search for the optimal point with two design variables. The difficulty arising from

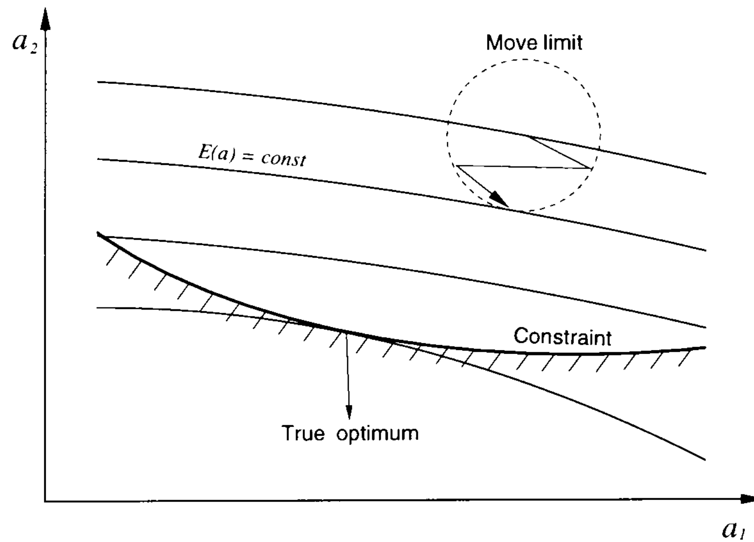

Fig. 3. Graphic representation of sequential linear programming.

the strong nonlinearity can be overcome by imposing a limit on $\delta\mathbf{a}$ indicated by a dotted circle in the figure. The optimal design variable $\delta\mathbf{a}$ is sought within this limit by the random search technique [16].

The optimum inlet velocity profile is determined under the constraints that the inlet flow rate is fixed and the velocity is nonnegative:

$$\int_{A_{\text{in}}} u_{\text{in}}\,\mathrm{d}A = \text{const} \tag{15}$$

$$u_{\text{in}}(r) \geq 0 \tag{16}$$

where A_{in} is the area of the reactor inlet. It can be readily shown, by simple rearrangement of the constant terms in the series (12), that Eq. (15) fixes the coefficient a_0 and no flow analysis for $k = 0$ is needed.

With the polynomial of 6th degree approximating the inlet velocity distribution, the optimization process converges in about 30 steps, each of which contains 4 flow-field calculations, for the most strongly nonlinear problem ($H = 1$, $Re = 100$) considered in this study; a diffusion dominant flow can get by with fewer flow analyses since milder nonlearity allows $\delta\mathbf{a}$ to take a larger step. It is evident that the use of a lager value for the limit on $\delta\mathbf{a}$ accelerates the convergence when converges. However, no attempt has been made in the present study to devise a systematic technique to find the optimal value. We used a sufficiently small limit (0.1–0.3) to get convergence without trial and error. The total computing time seems reasonable: about 180 min on a 233 MHz Pentium PC for the aforementioned problem.

4. Results and discussion

The flow-analysis code described in the earlier section was fully verified in Cho et al. [9], and the validation step will not be repeated here as the code is modified only slightly. A further evidence of the procedure is provided in Fig. 4 that shows the growth rate of GaAs epitaxial layer, which is normalized by the value at the center. The results are obtained for $Re = 13$, the rotation number $Re_{\Omega}/Re = 0.1$, and $H/R = 3$, with a nonuniformly distributed grid of 90×90. The computational results, which represent the concentration gradient normal to the surface, are

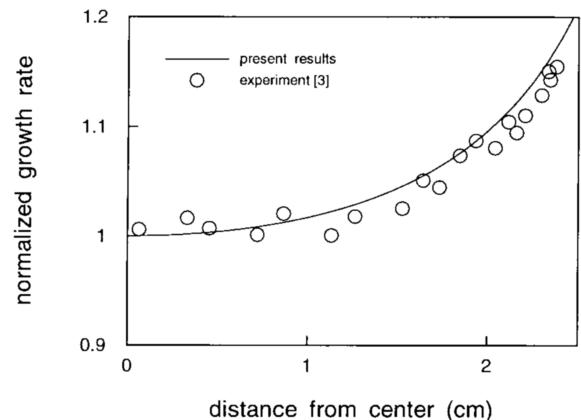

Fig. 4. Comparison of predicted and measured [3] growth rate in a vertical CVD reactor.

Table 1
Operating parameters employed in the present results

Height (H)	Re	Gr/Re^2	Cost function × 100		Average growth rate	
			uniform	optimum	uniform	optimum
1	1	0	5.3	2.2	1.5	1.6
1	10	0	3.0	0.32	3.6	4.1
1	100	0	4.4	0.22	11	15
0.5	1	0	1.1	0.31	2.4	2.4
0.5	10	0	0.58	0.029	5.0	5.1
0.5	100	0	1.5	0.11	15	17
1	10	50	25	5.9	4.0	4.4

in close agreement with the measurement taken by Wang et al. [3] and thus confirm that the code is functioning properly and is fit to be used in the optimization process. This also substantiates the earlier assumption that the growth rate is proportional to the normal concentration gradient.

We now turn the attention to the problem of optimizing the inlet velocity profile. The reactor performance depends greatly on the inlet flow rate which, for most MOCVD reactors, falls within the Re range of 0.1–100. The cases considered in the present study are for three different Reynolds numbers (Re = 1, 10, 100) in combination with two susceptor locations (H = 0.5, 1) as summarized in Table 1.

Owing to Fotiadis et al. [4], Pr and Sc for H_2 and $Ga(CH_3)_3$ as the working fluid (carrier gas) and the reactant gas at 900 K and 0.1 atm come out to be 0.7 and 2.33 since $\nu = 7 \times 10^{-3}$ (m^2/s), $\alpha_T = 1 \times 10^{-2}$ (m^2/s) and $\alpha_M = 3 \times 10^{-3}$ (m^2/s). A thorough test on the grid density and location of the exit plane in the exhaust passage has been carried out for the most convection dominant case, i.e. Re = 100, H = 1.0, with the uniform inlet flow. Table 2 compares the cost function and the average growth rate for various grids and domain sizes. It shows that these have converged and the relative errors in the results on coarse grids with respect to the value obtained with the finest grid (96 × 100) are very small. Also, since the results for a larger computational domain and those with a more strict convergence criterion (10^{-6}) are comparable, it is safe to conclude that the domain is large enough and

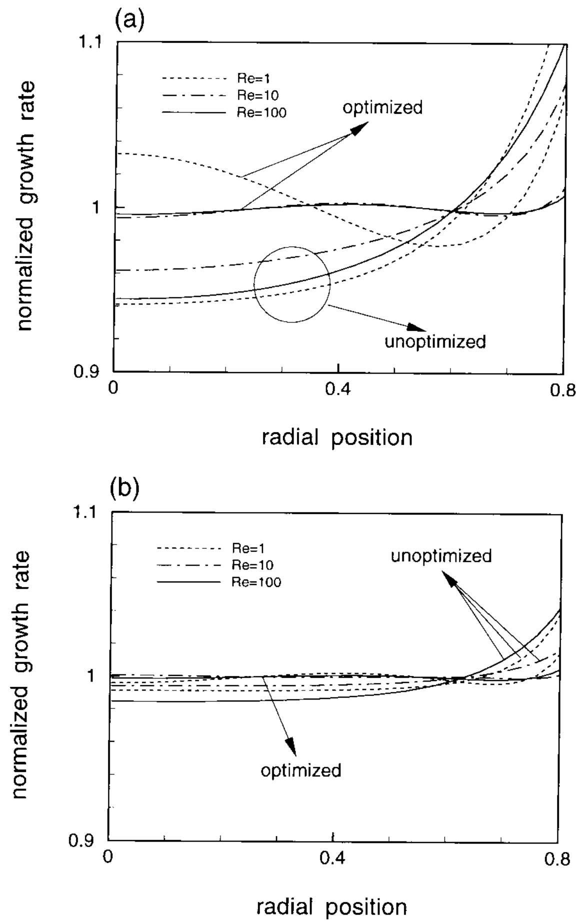

Fig. 5. Distribution of normalized growth rate as a function of radial position; (a) reactor height = 1, (b) reactor height = 0.5.

Table 2
Grid sensitivity on the function and average growth rate (H = 1, Re = 100)

Grid	Cost function E (×100)	Average growth rate	Remark
48 × 52	4.410 (1.2)[a]	11.27	
68 × 72	4.364 (0.14)[a]	11.27	selected
96 × 100	4.358	11.27	reference
68 × 72	4.367	11.27	(exit length) × 2
68 × 72	4.366	11.27	convergence, $\epsilon = 10^{-6}$

[a] ( ): relative error (%) with respect to the results of 96 × 100 grids.

the 68×72 grid is sufficiently fine to resolve the flow field and therefore are used throughout the study.

The growth-rate distribution normalized by its average value for various Reynolds numbers and two susceptor locations is shown in Fig. 5. The variation of the results in the radial direction for unoptimized uniform inlet flows is fairly large: the film is seen to grow faster in the outer part of the wafer while the growth rate is small and relatively uniform in the central region. The smaller than average growth rate near the center is attributed to the lack of replenishment of reactant as can be seen from the streamlines in Fig. 6; the accelerating flow near the susceptor edge, on the other hand, thins down the boundary layer and increases the growth rate. Also the variation is less for $Re = 10$ than for the other two Reynolds numbers, and this may be elaborated as follows. Comparing to the case for $Re = 10$, the mass transfer is enhanced by the stronger diffusion when $Re = 1$ and, hence, the reactant gas near the surface gets richer as it travels outward in the radial direction. On the other hand, the accelerating effects are more pronounced when $Re = 100$ due to the reduced flow passage resulting from a larger recirculation region seen in Fig. 6. It is interesting to note that the growth rate is more uniform for a smaller H (Fig. 5(b)) as the flow remains less disturbed because of a shorter travel distance.

To improve the uniformity of the growth rate for these cases, the optimization process, described in the previous section, is invoked to determine the inlet velocity profile. The resulting velocity distributions of 6th-degree Chebyshev polynomials are shown in Fig. 7 and the associated growth rates are compared in Fig. 5. It appears from the figure that the profiles for

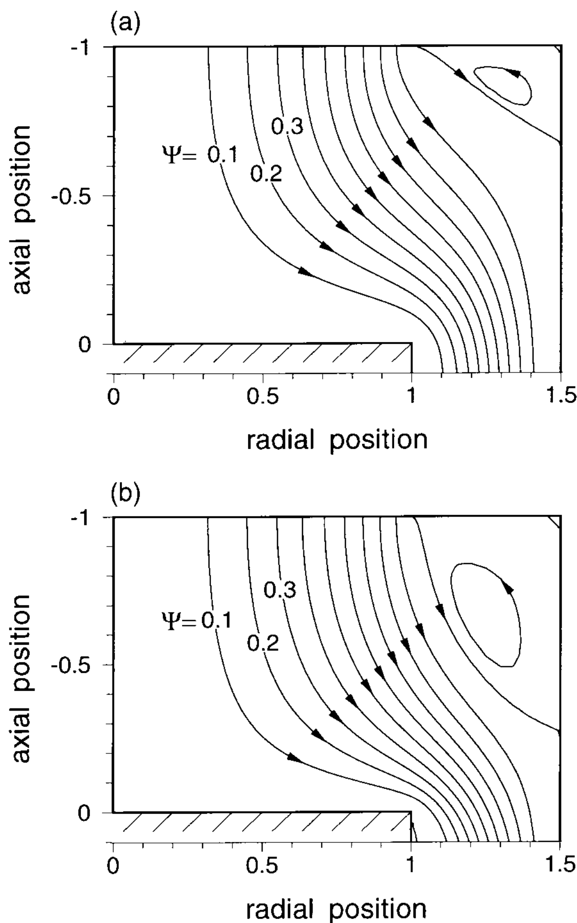

Fig. 6. Flow fields obtained with uniform inlet velocity; (a) $Re = 10$, (b) $Re = 100$.

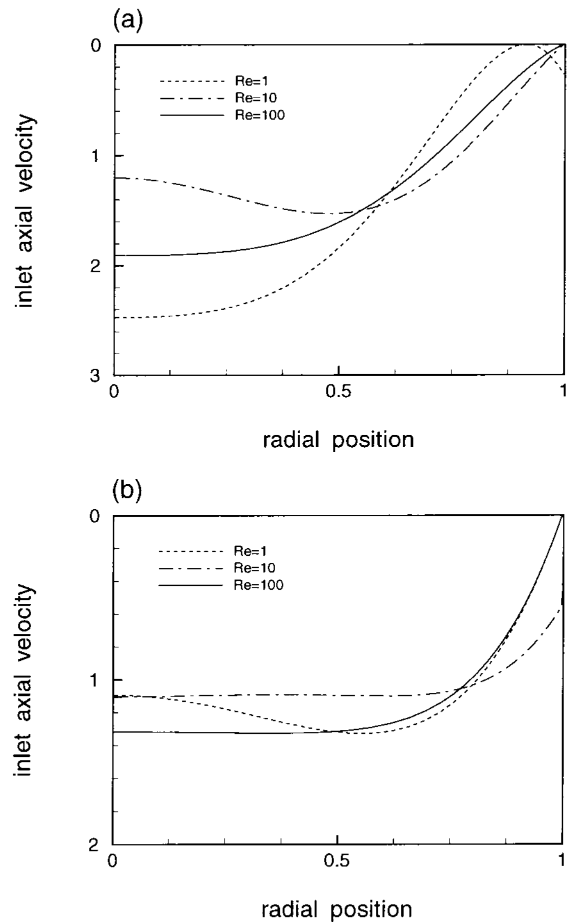

Fig. 7. Optimal inlet velocity profiles for various flow rates and reactor heights; (a) reactor height = 1, (b) reactor height = 0.5.

$H = 0.5$ are easier to produce than those for $H = 1$. It is because those for the latter vary substantially across the inlet cross-section. Note that, for both susceptor locations, the lowest Re case poses the most challenging optimization problem. The diffusion is so dominant in these cases and little can be altered by controlling the inlet profile especially when the distance to the susceptor face becomes large. The similar phenomenon was observed when the function to be optimized was the inlet concentration profile in Cho et al. [9].

The cost function and the average growth rate before and after the optimization are summarized quantitatively in Table 1. The improvement on uniformity is clear and remarkable; more than tenfold for $Re = 10$ and 100. The case for $Re = 1$ is not so successful, however, as the effective mixing due to diffusion nullifies any difference in inlet velocity profiles. The average growth rate also increases when the inlet velocity distribution is optimized. The trend is more pronounced with increasing Re. An interesting point may be drawn from this table. It is apparent that, between the two inlet-to-wafer distances, $H = 0.5$ is more efficient as could be expected in Fig. 5: the growth rate for unoptimized cases is higher (more efficient) and more uniform. The optimized inlet velocity distribution successfully narrows the gaps in growth rate and uniformity. This suggests that even if the chamber shape is not optimum, the performance may be brought close to optimum by controlling other parameters, such as the inlet velocity profile.

Figs. 8 and 9 depict the isovels for $H = 1.0$ and 0.5, respectively, for $Re = 100$ before (a) and after (b) the optimization. The axial velocity shows the clear trend of acceleration in the neighborhood of the susceptor corner when the inlet flow is uniform (a) as the fluid is squeezed to pass through the gap formed by the susceptor and the large recirculating region in the chamber corner. This inevitably thins the viscous layer on the wafer surface and increases the concentration gradient in the region as seen in Fig. 5. This situation can be improved by reducing the velocity in the inlet edge as plotted in Fig. 7. The corresponding isovels (Figs. 8(b) and 9(b)) become much more uniform as the flow nears the susceptor face.

As a final test case, we present the flow in which the buoyancy force is not negligible with $H = 1$, $Re = 10$, and $Gr/Re^2 = 50$. The flow and concentration fields along with the optimized inlet velocity profile are shown in Fig. 10. The streamlines for the uniform inlet velocity, which are denoted by the dotted lines, exhibit

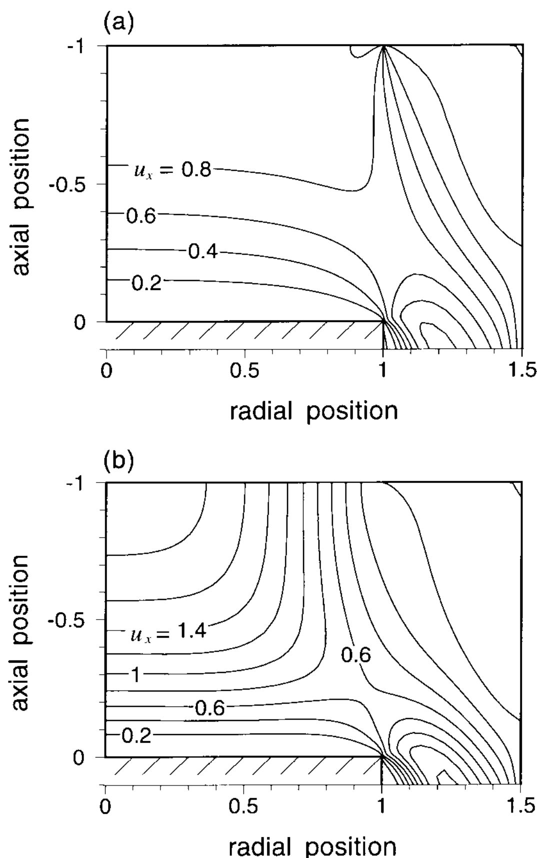

Fig. 8. Isovels of axial velocity component for $H = 1$ and $Re = 100$; (a) unoptimized, (b) optimized.

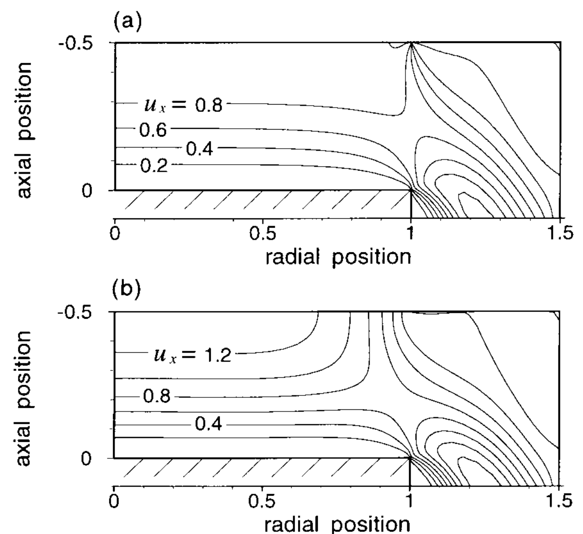

Fig. 9. Isovels of axial velocity component for $H = 0.5$ and $Re = 100$; (a) unoptimized, (b) optimized.

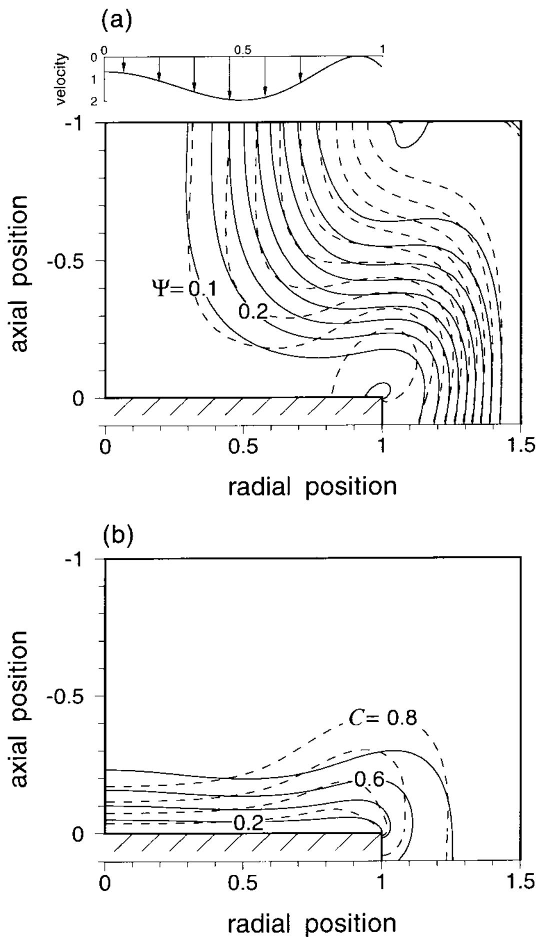

Fig. 10. Streamlines and concentration field for a mixed convection flow ($Gr/Re^2=50$), – –: unoptimized, —: optimized; (a) streamlines, (b) concentration field.

a sizable recirculating region near the susceptor corner. A large buoyancy driven upward motion is responsible for this and, as a result, the concentration gradient in the region decreases significantly and the uniformity suffers. The optimized inlet velocity is seen to reduce this undesirable phenomenon and greatly improves the growth-rate uniformity as the near parallel iso-concentration lines near the susceptor surface confirm.

5. Conclusions

The Navier–Stokes code developed earlier has been modified and incorporated in the present optimization technique for the inlet velocity profile to produce the most uniform epitaxial layer in a vertical MOCVD reactor for the given condition. The time-consuming nonlinear nature of the optimization process is efficiently handled by adopting the sequential linear programming approach.

The optimal inlet velocity profile represented by a 6th-degree Chebyshev polynomial is very successful in reducing the spatial non-uniformity of the growth rate. The procedure is particularly effective when the Reynolds number is high and the inlet-to-wafer distance becomes large. It is also found that a properly constructed inlet velocity profile can suppress the buoyancy driven secondary flow and improve the growth-rate uniformity. The present technique can be applied to find the optimal inlet-to-wafer distance and other shape optimization problems.

References

[1] K.F. Jensen, E.O. Einset, D.I. Fotiadis, Flow phenomena in chemical vapor deposition of thin films, Ann. Rev. Fluid Mech. 23 (1991) 197–232.

[2] P.D. Dapkus, Metalorganic chemical vapor deposition, Ann. Rev. Mater. Sci. (1982) 243–269.

[3] C.A. Wang, S. Patnaik, J.W. Caunt, R.A. Brown, Growth characteristics of a vertical rotating-disk OMVPE reactor, J. Crystal Growth 93 (1988) 228–234.

[4] D.I. Fotiadis, S. Kieda, K.J. Jensen, Transport phenomena in vertical reactors for metalorganic vapor phase epitaxy: effects of heat transfer characteristics, reactor geometry, and operating conditions, J. Crystal Growth 102 (1990) 441–470.

[5] S. Patnaik, R.A. Brown, C.A. Wang, Hydrodynamic dispersion in rotating-disk OMVPE reactors: numerical simulation and experimental measurements, J. Crystal Growth 96 (1989) 153–174.

[6] F. Durst, L. Kadinskii, M. Peric, M. Schafer, Numerical study of transport phenomena in MOCVD reactors using a finite volume multigrid solver, J. Crystal Growth 125 (1992) 612–626.

[7] D.I. Fotiadis, A.M. Kremer, D.R. McKenna, K.F. Jensen, Complex flow phenomena in vertical MOCVD reactors: effects on deposition uniformity and interfacial abruptness, J. Crystal Growth 85 (1987) 154–164.

[8] A.H. Dilawari, J. Szekely, A mathematical representation of a modified stagnation flow reactor for MOCVD applications, J. Crystal Growth 108 (1991) 491–498.

[9] W.K. Cho, D.H. Choi, M.-U. Kim, Optimization of inlet concentration profile for uniform deposition in a cylindrical chemical vapor deposition chamber, Int. J. Heat Mass Transfer 42 (1999) 1141–1146.

[10] P.N. Gadgil, Optimization of a stagnation point flow reactor design for metalorganic chemical vapor deposition by flow visualization, J. Crystal Growth 134 (1993) 302–312.

[11] M. Kondo, J. Okazaki, H. Sekiguchi, T. Tanahashi, S. Yamazaki, K. Nakajima, Highly-uniform large-area

MOVPE growing of InGaAsP by controlled stagnation point flow, J. Crystal Growth 115 (1991) 231–235.

[12] M. Kondo, A. Kuramata, T. Fujii, C. Anayama, J. Okazaki, H. Sekiguchi, T. Tanahashi, S. Yamazaki, K. Nakajima, An approach to versatile highly-uniform MOVPE growth: the flow controlled stagnation point flow reactor, J. Crystal Growth 124 (1992) 265–271.

[13] S.V. Patankar, Numerical Heat Transfer and Fluid Flow, McGraw-Hill, 1980.

[14] B.P. Leonard, A stable and accurate convective modelling procedure based on quadratic upstream interpolation, Computer Methods in Applied Mechanics and Engineering 19 (1979) 59–98.

[15] C.M. Rhie, W.L. Chow, A numerical study of the turbulent flows past an ioslated airfoil with trailing edge separation, AIAA Journal 21 (1983) 1525–1532.

[16] G.N. Vanderplaats, Numerical Optimization Techniques for Engineering Design, McGraw-Hill, 1984.